Determination of Ice Water Path and Mass Median Particle Size Using Multichannel Microwave Measurements

GUOSHENG LIU

Department of Meteorology, The Florida State University, Tallahassee, Florida

JUDITH A. CURRY

Program in Atmospheric and Oceanic Sciences, University of Colorado, Boulder, Colorado

(Manuscript received 28 June 1999, in final form 23 September 1999)

ABSTRACT

The method of simultaneously retrieving ice water path and mass median diameter using microwave data at two frequencies is examined and implemented for tropical nonprecipitating clouds. To develop the retrieval algorithm, the authors first derived a bulk mass–size relation for ice particles in tropical clouds based on microphysical data collected during the Central Equatorial Pacific Experiment. This relation effectively allows ice particle density to decrease with particle size. In implementing the retrieval algorithm, 150- and 220-GHz Millimeter-Wave Imaging Radiometer data collected during the Tropical Ocean and Global Atmosphere Coupled Ocean–Atmosphere Response Experiment were used. Ice water path and mass median diameter are determined based on a lookup table generated by a radiative transfer model. The lookup table depends on cloud type, cloud liquid water path, and atmospheric temperature and humidity profiles. Only nonprecipitating clouds are studied in this paper. Error analyses were performed by a Monte Carlo procedure in which atmospheric profiles, ice cloud height, liquid water content, surface temperature, and instrument noise vary randomly within their uncertainty range through a Latin hypercube sampling scheme. The rms error in the retrievals is then assessed and presented in a two-dimensional diagram of ice water path and mass median diameter. It is shown that the simultaneous retrieval method using 150 and 220 GHz may be used for clouds with ice water path larger than 200 g m^{-2} and mass median diameter larger than 200 μm. To obtain meaningful retrievals for ''thinner'' clouds, higher microwave frequencies are needed. It is also shown that liquid water clouds that are at the same altitude as ice clouds interfere with the retrievals to a significant degree. To obtain reasonable ice water path and mass median size retrievals, it is necessary first to group clouds into several classes, then to apply separate algorithms to the different classes. The accuracy of the retrievals also depends on cloud type, with the best accuracy for cirrus and the worst for the midtop mixed-phase cloud among the clouds investigated in this study.

1. Introduction

The amount of condensed water in ice clouds is one of the most important physical parameters in determining the earth's radiation balance. The reflection of shortwave radiation by ice clouds reduces the solar energy reaching the earth's surface. High-altitude ice clouds also have a ''greenhouse effect'' because their cold temperatures permit less infrared radiation to escape to space than under clear-sky conditions. The complex effect of ice clouds on the earth's radiation budget has been discussed by Liou (1986). Knowledge of ice water content is essential to infer cloud vertical structure (e.g., Sheu et al. 1997), which determines the cloud vertical heating profile, and to parameterize ice cloud radiative properties for general circulation models (e.g., Heymsfield and Donner 1990; Ebert and Curry 1992; Fu and Liou 1993).

Studies of cloud ice water content have previously been conducted primarily using aircraft in situ measurements (e.g., Knollenberg et al. 1993; Heymsfield 1993). Recently, Heymsfield and McFarquhar (1996) and McFarquhar and Heymsfield (1996) investigated the microphysical characteristics and radiative properties of tropical cirrus using aircraft-measured data during the Central Equatorial Pacific Experiment (CEPEX). In order to understand the large-scale characteristics of ice water distribution, remote sensing is desirable. However, retrievals of ice water from remotely sensed data are still in the development stage. Minnis et al. (1993a,b) developed a method to retrieve cirrus cloud properties from satellite-observed visible and infrared data. The visible–infrared method cannot distinguish between ice and liquid cloud water. Ground-based remote sensing of ice water content using radar and infrared radiometer

Corresponding author address: Guosheng Liu, Department of Meteorology, The Florida State University, Tallahassee, FL 32306-4520. E-mail: liug@met.fsu.edu

was proposed by Matrosov et al. (1992, 1994). Using satellite and airborne radiometer data, ice water path (IWP) over oceans was retrieved by Lin and Rossow (1994, 1996), Sheu et al. (1997), Liu and Curry (1998, 1999), and Deeter and Evans (2000). Lin and Rossow estimated IWP as the residual of visible-derived total water path minus microwave-derived liquid water path. Sheu et al. pursued the same approach for layered clouds but added ''dense ice'' contribution derived from Special Sensor Microwave Imager (SSM/I) data for deep precipitating clouds. Liu and Curry (1998, 1999) estimated IWP from the scattering signatures in high-frequency microwave channels in the Special Sensor Microwave Water Vapor Sounder (SSM/T-2) and airborne Millimeter-Wave Imaging Radiometer (MIR). In their retrievals, particle size was not retrieved but rather specified empirically based on cloud temperature.

By analyzing the error sources, Liu and Curry (1998) concluded that the uncertainty in particle size and the existence of liquid water in and above the ice cloud layer contribute most of the error in the IWP retrievals. Liu and Curry (1999) included liquid water path estimated from SSM/I in their SSM/T-2 IWP algorithm to take into account the influence of cloud liquid. However, the particle size effect still remains unresolved in their retrieval algorithm. Based on results of radiative transfer simulations, Evans and Stephens (1995a,b) first suggested the possibility of retrieving ice water path and mass median particle size simultaneously using data at two microwave frequencies. Their study was based on radiative transfer model simulations of cirrus clouds. A subsequent (also theoretical) study by Evans et al. (1998) further discussed the accuracy of this approach when using two submillimeter microwave frequencies (630 and 880 GHz). Weng and Grody (1998) also proposed a similar approach based on a two-stream approximation of radiative transfer model solution. Wang et al. (1998) showed that both particle size and ice water path should, in principle, be simultaneously retrievable from MIR data although they did not develop an actual algorithm. Deeter and Evans (2000) pursued this approach for 150- and 220-GHz MIR data collected during the Tropical Ocean and Global Atmosphere Coupled Ocean–Atmosphere Response Experiment (TOGA COARE) (Webster and Lukas 1992). In their study they excluded all cases possibly ''contaminated'' by liquid water or rain, which results in their algorithm being able to be applied to only 0.15% of the total observed pixels.

In this study we further explore the idea of simultaneously retrieving IWP and particle size using multiple microwave frequencies. In particular, we apply a cloud classification scheme to divide observed pixels into several cloud types and then use separate algorithm configurations for different cloud types. This cloud classification makes it possible for us to understand to what portion in the whole cloud spectrum the retrieval algorithm can be used and to what portion it cannot. Additionally, this study also differs from that of Deeter and Evans (2000) primarily in the following two aspects: First, we use ice particle mass, density, and size distribution relations directly derived from in situ measurements in the Tropics during CEPEX. Second, we expand the retrievals to clouds that may also contain cloud liquid water, which allows us to dramatically increase the number of ''retrievable'' cloud pixels. Only nonprecipitating clouds are considered in this study.

2. Analyzing the mass, density, and size distribution of ice particles

In developing IWP retrieval algorithms, a realistic representation of ice particles in radiative transfer models is needed. In this section, we describe how the ice particles are treated in our radiative transfer models. By analyzing microphysical data collected from CEPEX, McFarquhar and Heymsfield (1996) found that there was a wide variety of crystal habits in the same cloud and there was substantial variation of crystal types in the horizontal and vertical. Therefore, within one radiometer's field of view, a cloud can contain many different ice particle habits. Using one nonspherical shape for one ''scene'' in the radiative transfer model is not necessarily superior to just assuming all particles being spheres, which allows much simpler mathematical representation. For this reason, we use an equal-mass sphere to represent an ice particle and allow the ice particle density to vary with its size. Observational evidence shows that the mass (M) of ice particles may be expressed by power laws of the particles' longest dimension (L) (cf. Mitchell 1996):

$$M = \alpha L^{\beta}, \tag{1}$$

where α and β depend on the habits and the sizes of the ice particles. The αs and βs for 14 ice particle shapes based on available data published in the literature were summarized by Mitchell (1996).

As mentioned above, there could be several types of ice particles within a single field of view of the radiometer. Here, we try to derive an overall relation between M and L, which takes the average over all the existing ice particle types in a cloud. To derive this overall relation, we use the microphysical data collected by a Particle Measuring Systems (PMS) two-dimensional cloud probe (2DC) during CEPEX. The 2DC measures the two-dimensional image of ice particles with longest dimensions from 30 to 3000 μm. Particle masses were determined following Heymsfield et al. (1990) based on the dimensions and area ratio of two-dimensional images. A more detailed description of the procedure has been given by McFarquhar and Heymsfield (1996). The data have been archived at the CEPEX Integrated Data System located at University of California, San Diego. The archived data were arranged into 28 bins based on their longest dimension. In each bin the total mass and the number concentration were reported in every 10 s. Here, we calculated the mass of

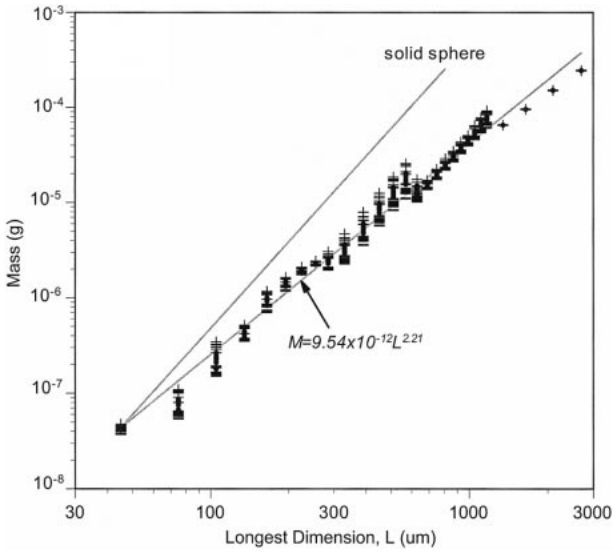

FIG. 1. The relationship between mass (M) and the longest dimension (L) derived for ice particles collected during CEPEX. Solid dots (●) are mean values, and "+" and "−" are the mean plus or minus one standard deviation, respectively. A curve for solid sphere is shown for reference. The best-fitting curve (2) is also shown.

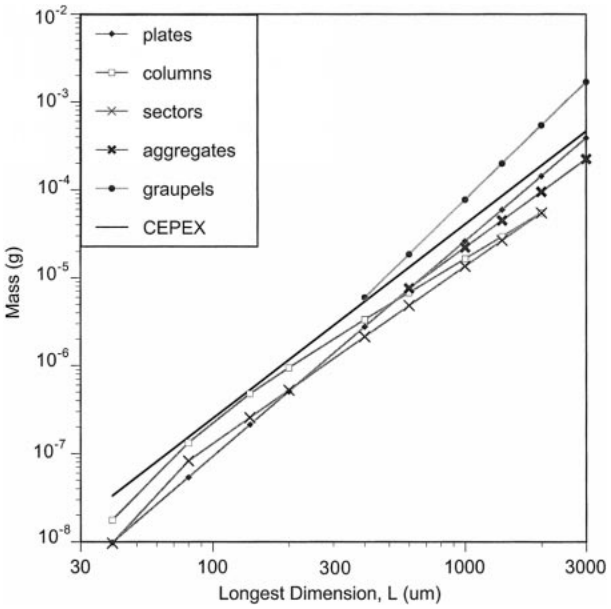

FIG. 2. Comparison of the mass–size relation among several different ice particle shapes. "CEPEX" is derived from this study; others are based on Mitchell (1996).

a particle by dividing the total mass with number concentration within a bin during l0 s. Using all the data collected during CEPEX (7 March–5 April 1993), we calculated the mean and standard deviation of the particle mass in each bin. In making these calculations, we further grouped the data into eight different temperature ranges from 0° to −80°C by every 10°C interval, in order to examine whether there is a temperature dependence.

The relationship between mass and the longest dimension derived based on the aforementioned procedure is shown in Fig. 1, in which solid dot (●) denotes the mean mass, "+" and "−" denote the mean plus or minus one standard deviation, respectively. Results for all eight temperature ranges are plotted, but they are very close to each other. That is, the temperature dependence of the M–L relation is insignificant, especially for larger ice particles. In addition, the standard deviation, which reflects the scatter among different samples, is also small (less than 30% of the mean). Therefore, we choose a fixed pair of α and β to represent the overall M–L relation, which reflects the average over all kinds of ice particles found in the tropical cirrus clouds. A best fit of data in Fig. 1 gives

$$M = 9.54 \times 10^{-12} L^{2.21}, \tag{2}$$

where M is in grams and L is in micrometers. This relation is used in our radiative transfer model. In Fig. 2 we compare the M–L relation derived here (called "CEPEX") with several others given in Mitchell (1996). It is seen that the CEPEX M–L relation is close to columns for smaller particles and plates for larger particles. It generally gives a greater mass for the same L than other M–L relations except for graupels. Because most of the data used in Mitchell (1996) came from midlatitudes, the greater values of mass by the CEPEX M–L relation may imply that ice particles in the tropics are generally denser than those in midlatitudes. Equation (2) effectively allows the ice particle's bulk density to decrease with its size, which is consistent with observational evidence (cf. Pruppacher and Klett 1997).

Based on all available CEPEX 2DC data, Liu and Curry (1998) found that the ice particle size distribution may be expressed by

$$N(L) = \begin{cases} N_0 \left(\dfrac{100}{L}\right)^{3.5} & L \le 100\ \mu\text{m}, \\ N_0 \exp\left[-5\left(\dfrac{L-100}{L_{\text{mm}}+500}\right)^{0.75}\right], & L > 100\ \mu\text{m}, \end{cases} \tag{3}$$

where $N(L)$ is the number concentration ($\text{m}^{-3}\ \mu\text{m}^{-1}$), N_0 is a constant that corresponds to the ice number concentration at 100 μm, and L_{mm} is the mass median value of L (μm) by which ice particles are divided into two groups with equal mass. In this study, we use mass-equivalent spheres of solid ice in our radiative transfer model. The diameter of the mass-equivalent sphere D can be related to L by

$$D = 2.71 L^{0.737}, \tag{4}$$

which is derived from (2) by assuming that the density of solid ice is 0.916 g cm^{-3}. Similar to L_{mm}, we define a mass median diameter D_{mm}, which is the mass median value of D and is also related to L_{mm} through (4).

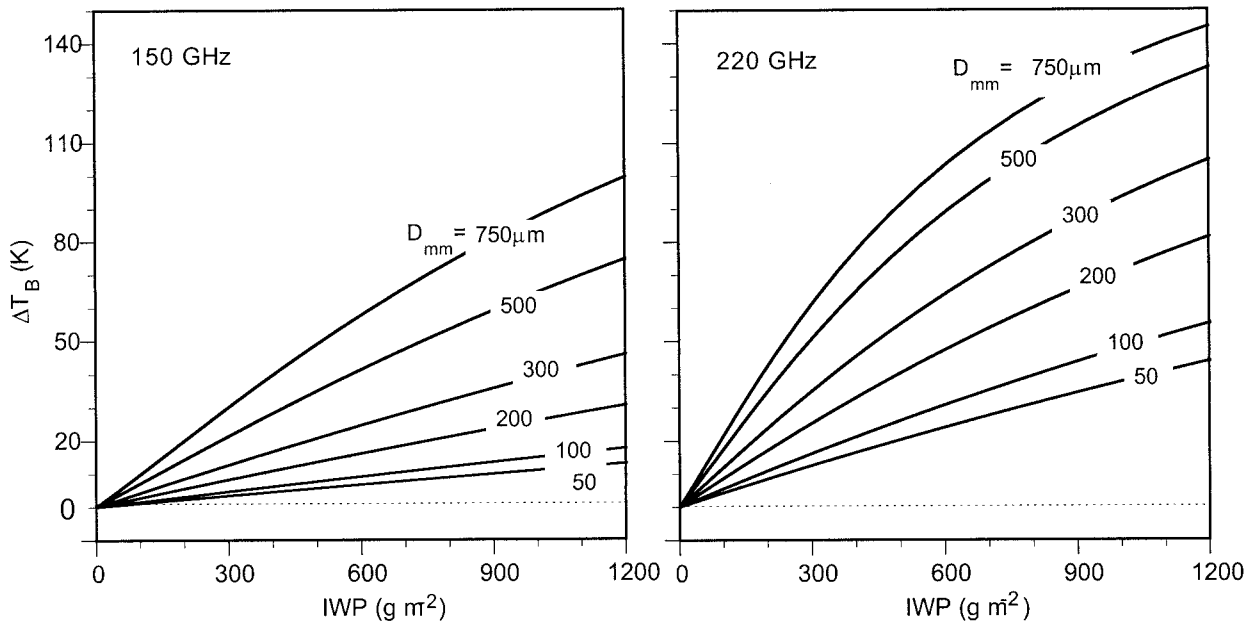

FIG. 3. Brightness temperature depression (ΔT_B) vs IWP for 150- and 220-GHz frequencies as simulated by a radiative transfer model.

3. Retrievals of ice water path and mass median diameter

a. Radiative transfer model results

A radiative transfer model using 32-stream discrete ordinate method (Liu and Curry 1993; Liu 1998) is used to investigate the radiative properties of ice clouds. In these model simulations we use a standard tropical atmosphere profile and a calm ocean surface (no wind) with temperature of 300 K. The surface emissivity model of Klein and Swift (1977) is used for the no-wind condition. Figure 3 shows the brightness temperature depressions relative to clear sky ($\Delta T_B = T_{\mathrm{BCLR}} - T_B$, where T_B is cloudy sky brightness temperature and T_{BCLR} is clear-sky brightness temperature) versus IWP for 150 and 220 GHz. These frequencies are available on the airborne radiometer MIR whose data are used in this study. An ice cloud located from 9 to 10 km is assumed, and mass median diameter, D_{mm} varies from 50 to 750 μm. It is seen that particle size affects the IWP–ΔT_B relation significantly, which was also pointed out earlier by Evans and Stephens (1995b) and Liu and Curry (1998). As suggested by Evans and Stephens (1995b), since the particle size effects on ΔT_B depend on microwave frequency, the ratio of ΔT_Bs at two different frequencies may contain particle size information. Figure 4 shows the ΔT_B ratio of 220 over 150 GHz ($\Delta T_{\mathrm{B220}}/\Delta T_{\mathrm{B150}}$). The ratio varies from 1.5 to 4 depending on both D_{mm} and IWP, the smaller value of IWP or D_{mm} corresponding to a larger ratio.

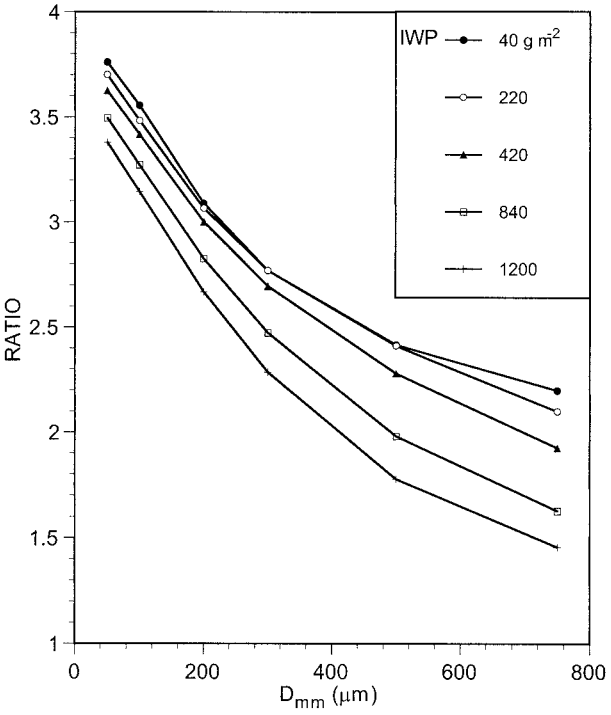

FIG. 4. Brightness temperature depression ratio ($\Delta T_{\mathrm{B220}}/\Delta T_{\mathrm{B150}}$) vs mass median diameter (D_{mm}) as simulated by a radiative transfer model.

Therefore, we may retrieve IWP and D_{mm} simultaneously from ΔT_{B220} and $\Delta T_{\mathrm{B220}}/\Delta T_{\mathrm{B150}}$, as illustrated in Fig. 5, in which the isolines of IWP and D_{mm} are plotted using the model results as mentioned above. In the retrieval algorithm, this diagram serves as a two-dimensional lookup table. Once ΔT_{B220} and $\Delta T_{\mathrm{B220}}/\Delta T_{\mathrm{B150}}$ are derived from radiometer data, one can find IWP and D_{mm} from this table. Our model simulation suggests that a diagram using a combination of 89 and 150 GHz may be used for very deep ice clouds or precipitating clouds.

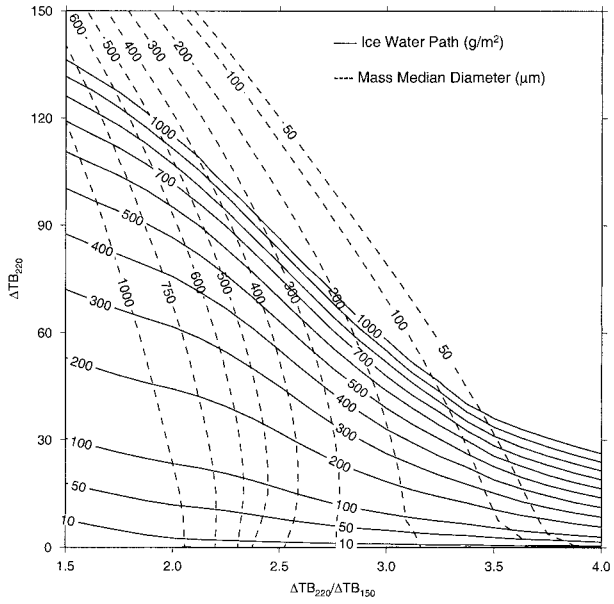

FIG. 5. Isolines of IWP and D_{mm} in the 2D diagram of ΔT_{B220} and $\Delta T_{B220}/\Delta T_{B150}$ generated from results of a radiative transfer model. This diagram conceptually illustrates the simultaneous retrieval algorithm of IWP and D_{mm}.

Similarly, for thin cirrus clouds, the combination of 220 and 340 GHz would be preferable because of their higher sensitivities to small ice particles. All the frequencies mentioned here are available on the MIR. In addition, 92- and 150-GHz channels are also available in SSM/T-2 and the Advanced Moisture Sounding Unit-B of *NOAA-K* and later satellites.

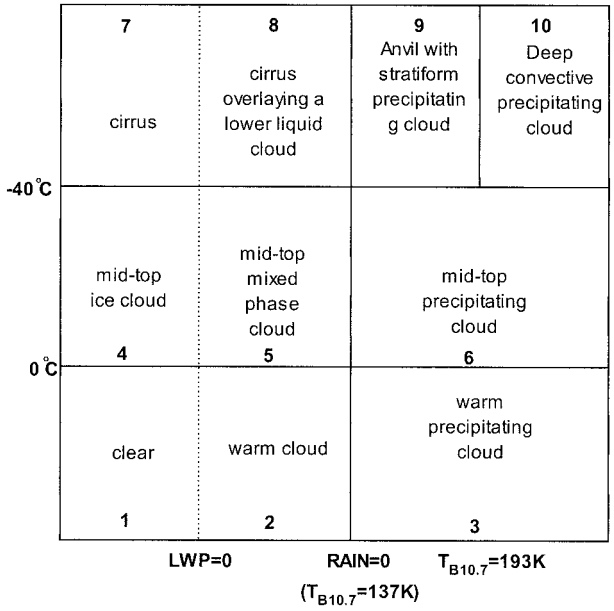

FIG. 6. Conceptual diagram of cloud classification as adapted from Liu and Curry (1998).

b. Data sources

The primary data sources are MIR brightness temperatures, with the Moderate-Resolution Imaging Spectroradiometer Airborne Simulator (MAS) and the Advanced Microwave Precipitation Radiometer (AMPR) measurements used as ancillary data. All three instruments were onboard the NASA ER-2 aircraft during TOGA COARE. The MIR is a cross-scan radiometer operating at seven frequencies: 89, 150, 183.3 ± 1, 183.3 ± 3, 183.3 ± 7, 220, and 340 GHz (Racette et al. 1996; Wang et al. 1997). Data from 340 GHz are not available during TOGA COARE. The sensitivity of the MIR frequencies to ice clouds was first modeled by Gasiewski (1992). The MIR scans ±50° from nadir every 3 s, during which unpolarized radiances at 57 positions are sampled. Beamwidth of MIR channels are 3.5°, which corresponds to 1.2 km at nadir when the aircraft flies at an altitude of 20 km. For better collocation with MAS and AMPR, we only use data within ±15° of nadir in this study, although the algorithm is capable of being applied at other viewing angles. The brightness temperature sensitivity is about 1 K for any of the MIR channels. The AMPR is a four-channel cross-scanning microwave radiometer with frequencies at 10.7, 19.35, 37.1, and 85.5 GHz (Spencer et al. 1994). The spatial resolution at nadir is about 2.8 km for 10.7 GHz and 0.6 km for 85.5 GHz. AMPR data are used to determine liquid water path and the presence of rain. MAS has 12 channels ranging from visible to infrared (King et al. 1996) with a nadir resolution of about 50 m. Here we use the 12-μm channel radiance to calculate cloud-top temperature for determining cloud type. For geocollocation of MIR, AMPR, and MAS data, we choose the nearest AMPR and MAS pixels to match MIR pixel. Because of their different resolutions, the sensors do not have the same field of view. In addition, atmospheric temperature and humidity profiles from the European Centre for Medium-Range Weather Forecasts (ECMWF) analyses are used as radiative transfer model inputs for creating the retrieval lookup tables. ECMWF data are available twice daily (0000 and 1200 UTC) at 2.5° × 2.5° spatial resolution.

c. Description of retrieval algorithm

The lookup diagram as shown in Fig. 5 varies with many factors, including atmospheric temperature and humidity profiles, the altitude of the ice clouds, surface emissivity, and the presence of liquid water clouds. Of these factors, cloud liquid within the ice cloud layer significantly alters the lookup table since emission from liquid water directly reduces the ice-scattering signature (Liu and Curry 1998, 1999). Therefore, ancillary data on cloud liquid water are needed for the IWP retrieval algorithm. In this study, we first group observed clouds into several types using a cloud classification scheme developed by Liu et al. (1995) and slightly modified by

Liu and Curry (1998) as shown in Fig. 6. This cloud classification uses cloud-top temperature determined by MAS, and liquid water path and rain intensity estimated from AMPR. The AMPR 10.7-GHz brightness temperature is used for the rain threshold ($T_{B10.7} > 137$ K) and for separating light and heavy precipitating clouds (Liu and Curry 1998). In this cloud classification scheme, there are 10 cloud types, with 7 having cloud-top temperatures colder than 0°C. Furthermore, of the cold clouds three cloud types are precipitating. Although IWP and D_{mm} in precipitating clouds may be retrieved using a combination of 89 and 150 GHz, it requires knowledge of vertical profiles of rain, which we leave for further study. Therefore, the following four cloud types are considered in this study: cirrus, midtop ice cloud, cirrus overlaying a lower liquid water cloud, and midtop mixed phase cloud.

For each observed pixel, the algorithm first determines the cloud class according to Fig. 6. Pixels that fall into the categories other than the aforementioned four are excluded from the retrieval process. About 58% of the total collocated pixels are excluded from this filtering, of which 11% are clear sky, 10% are warm clouds, and 37% are cold precipitating clouds. Cloud liquid water path is also required in the cloud classification, for which we incorporated the microwave data from AMPR. A liquid water path algorithm adapted from Liu and Curry (1993) is applied to AMPR's 19.35- and 37.1-GHz frequencies (both frequencies are similar to those on Special Sensor Microwave Imagers). If the algorithm determines no liquid water, the cloud is classified to be cirrus or midtop ice cloud depending upon its cloud-top temperature. Otherwise, the cloud is classified to be either cirrus overlaying a lower liquid water cloud or midtop mixed-phase cloud. The retrieval of total liquid water path is partitioned into low- and mid-cloud layers using a ''cloudiness likelihood'' (Sheu et al. 1997) based on ECMWF vertical relative humidity profile. A detailed description of the partition is given in Liu and Curry (1999).

A fast radiative transfer model (Liu 1998) is used to create a lookup table similar to Fig. 5 for each MIR pixel using ECMWF atmospheric profiles (at the closest model grid and time) and the aforementioned cloud liquid water configuration. For cirrus and cirrus overlaying a lower liquid water cloud, the ice cloud layer is assumed to be between 100 and 200 mb (approximately 12–16 km). For midtop ice and midtop mixed-phase clouds, the ice cloud layer is assumed to be between 300 to 500 mb (approximately 6–9 km). Then, IWP and D_{mm} are derived from the lookup table using ΔT_{B220} and $\Delta T_{B220}/\Delta T_{B150}$. As shown in Fig. 5, ΔT_{B220} loses its sensitivity to IWP when $\Delta T_{B220}/\Delta T_{B150}$ exceeds ~3.25, or $D_{mm} < \sim 150$ μm. For these cases, small uncertainty in ΔT_B causes a large variation in $\Delta T_{B220}/\Delta T_{B150}$. Therefore, the simultaneous retrieval of IWP and D_{mm} is no longer meaningful. More discussion is given to these ''thin'' ice clouds in the error analyses section. Deeter and Evans (2000) also did not perform retrievals for cases with D_{mm} less than 200 μm. For these cases, instead of retrieving both IWP and D_{mm} from the two-dimensional lookup table (referred to as 2D retrieval, hereinafter), we only retrieve IWP using the statistical method described by Liu and Curry (1998) (referred to as 1D retrieval, hereinafter). The 1D algorithm uses an empirical relation between cloud temperature and particle mass median diameter derived from CEPEX data. Based on radiative transfer simulations, IWP is related to brightness temperature depressions at 150 and 220 GHz. Uncertainties in particle size and supercooled liquid water amount are the major error sources. A rough estimate indicates that possible error by uncertainty in particle size is at least 50%, and by uncertainty in supercooled liquid waters is at least 30%.

TABLE 1. Statistics of pixel numbers used in the retrieval algorithm.

	Midtop ice cloud	Midtop mixed-phase cloud	Cirrus	Cirrus with liquid water cloud
2D retrievals	1010	2364	8595	17 273
1D retrievals	14 264	65 732	10 529	33 097
No detectable ice	35 417	30 631	7533	13 345
Total	50 691	98 727	26 657	63 715

d. Retrieved IWP and D_{mm} statistics

The retrieval algorithm is applied to MIR data collected in 12 ER-2 flights during TOGA COARE. In Table 1 we list the pixel numbers that meet the requirements for the 2D retrieval ($\Delta T_{B220} > 0$, $\Delta T_{B150} > 0$, and $\Delta T_{B220}/\Delta T_{B150} < 3.25$), that only meet the requirements for the 1D retrieval ($\Delta T_{B220} > 0$ and $\Delta T_{B150} > 0$), and that have no detectable ice ($\Delta T_{B220} \leq 0$ or $\Delta T_{B150} \leq 0$). No 2D retrieval is performed for observations with $\Delta T_{B220}/\Delta T_{B150} > 3.25$. It is seen that the 2D retrieval can be applied to about 30% of the high clouds (cirrus and cirrus overlaying a lower liquid water cloud); it can only be applied to about 2% of mid clouds. Note these numbers are still significantly higher than the 0.15% that passed the filter of Deeter and Evans (2000). Figure 7 shows the frequency distributions of (a) IWP determined by the 2D retrieval algorithm, (b) D_{mm} determined by the 2D retrieval algorithm, (c) IWP determined by the 1D retrieval algorithm (excluded by 2D retrieval algorithm), and (d) IWP determined by combined 2D and 1D retrievals (all retrievals), for the four different cloud classes. The mean and standard deviations of these retrievals are listed in Table 2. Cases with no retrieved IWP are not included in the diagrams. If we consider all IWP retrievals (Fig. 7d), the frequency of the IWP values decreases with increasing IWP for all the cloud classes except for cirrus, which shows a secondary maximum near 150 g m^{-2}. The result is consistent with earlier studies (Lin and Rossow 1996; Liu and Curry

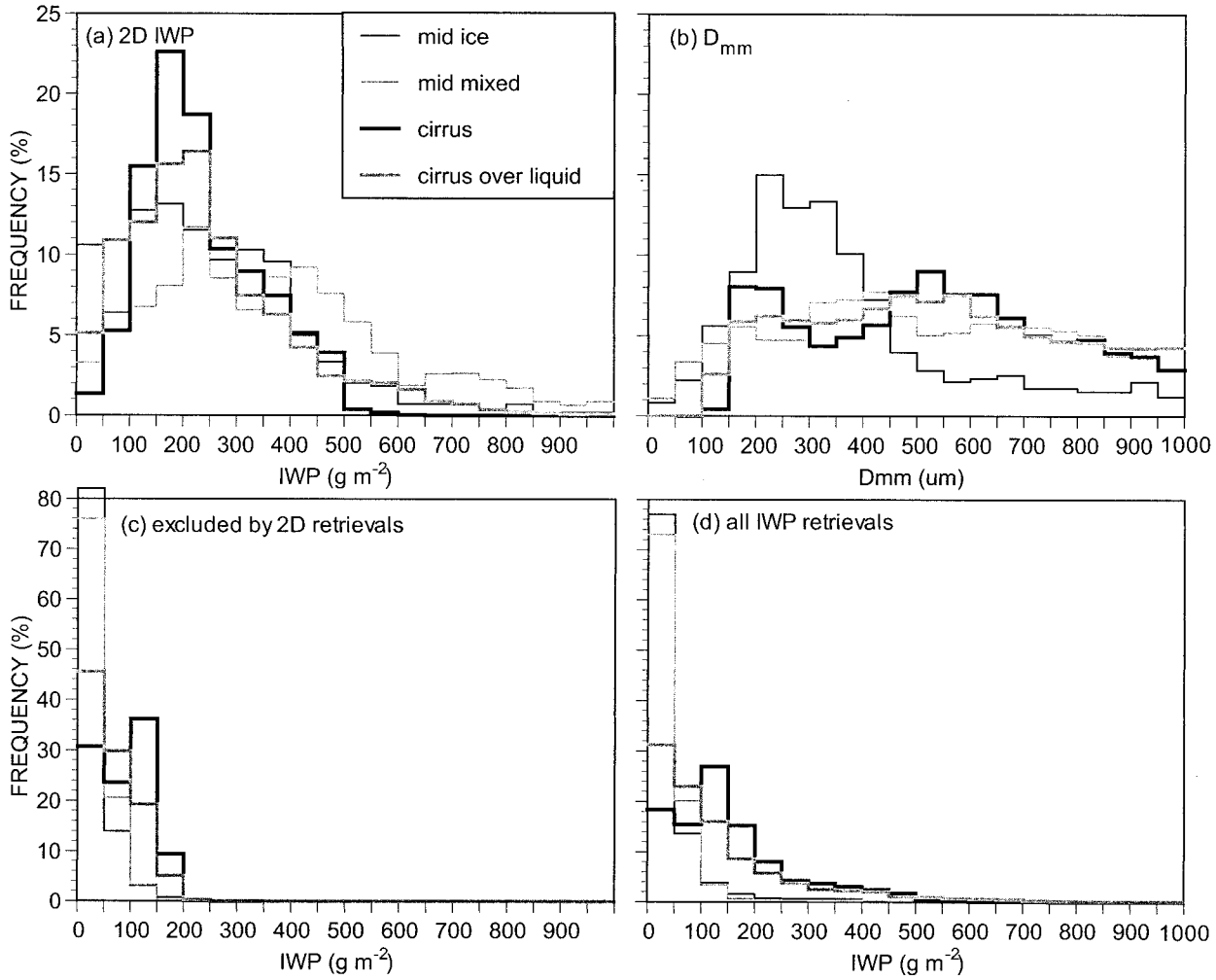

FIG. 7. Frequency distributions for all four cloud types of (a) IWP determined by the 2D retrieval algorithm, (b) D_{mm} determined by the 2D retrieval algorithm, (c) IWP determined by the ID retrieval algorithm (excluded by the 2D algorithm), and (d) IWP determined by combined 2D and 1D algorithms (all retrievals).

1998, 1999). The 2D retrievals are done for the clouds with D_{mm} generally larger than 150 μm. Therefore, when interpreting the 2D retrieval results, we should keep in mind that the retrievals only contain information on clouds with large ice particles. The clouds that were missed by the 2D retrievals have smaller ice particles and lower IWPs.

For midtop ice clouds, the results show that most of IWPs are less than 50 g m^{-2}. Clouds for which the 2D retrieval algorithm can be applied showed IWP values generally less than 500 g m^{-2} and D_{mm} values less than 500 μm. The maximum frequency of D_{mm} is around 250 μm, just above the low limit detectable by the 2D retrieval algorithm. Considering that the clouds missed by the 2D retrievals consist of smaller particles, the mode D_{mm} for ''all midtop ice clouds'' is most likely less than 200 μm. On the other hand, for cirrus clouds, which have colder cloud tops than midtop ice clouds, there seems to be a secondary D_{mm} mode near 500 μm besides the mode likely smaller than 200 μm (for the same reason given to midtop ice cloud, we believe that there is a mode of D_{mm} smaller than 200 μm). The double-mode feature in the D_{mm} distribution can also be seen in cirrus overlaying a lower liquid water cloud. It is interesting that a secondary mode near 500 μm can also be found in the CEPEX in situ data (as shown in Fig. 8). The secondary mode in CEPEX data seems to be several tens of microns smaller than that in MIR retrievals. The reason for the secondary mode near 500 μm is not clear to the authors. However, because of their high tops, the cirrus and cirrus overlaying lower liquid water clouds could be very deep and/or multilayer. Possible large precipitating ice particles in these clouds could have produced the mode near 500 μm.

4. Error analyses

Uncertainties in the following variables cause error in the IWP and D_{mm} retrievals: cloud liquid water, pre-

TABLE 2. Mean and standard deviation of retrieved IWPs (g m^{-2}) and D_{mm}s (μ).

	Mean	Std dev
Midtop ice cloud		
2D IWP	255	170
D_{mm}	368	208
IWPs excluded by 2D	29	30
All IWPs	43	75
Midtop mixed-phase cloud		
2D IWP	362	213
D_{mm}	502	253
IWPs excluded by 2D	38	28
All IWPs	49	76
Cirrus		
2D IWP	235	107
D_{mm}	530	230
IWPs excluded by 2D	87	51
All IWPs	151	111
Cirrus over liquid water cloud		
2D IWP	250	159
D_{mm}	534	239
IWPs excluded by 2D	66	46
All IWPs	136	142

cipitable water, ice cloud height, air temperature, surface wind, and sensor noise. In this section we study the error in IWP and D_{mm} retrievals caused by these uncertainties using a Monte Carlo procedure. In Table 3, we list the uncertainty range for each variable allowed in the Monte Carlo study. The uncertainty for liquid water path is based on Liu and Curry (1993). The variation of tropospheric air temperature profile in the Tropics is very small, typically less than 1°C. The sensors' noises are based on MIR specification (Wang et al. 1997). The uncertainty of precipitable water in ECMWF analyses is not clear; the value ($\pm$10 kg m^{-2}) used here is somewhat arbitrary. In calculating sea surface emissivity for windy conditions, the emissivity model proposed by Schluessel and Luthardt (1991) was used. In performing the Monte Carlo study, we first perturb each variable within its allowed range from its baseline value. The magnitude of perturbation is chosen by a Latin hypercube sampling method, which is more efficient than simple random sampling method in selecting input values for Monte Carlo procedures (McKay et al. 1979). We divide the entire error range for each variable into 16 intervals with equal possibility, and one value is drawn at random from each interval. Then they are matched at random for the seven input variables listed in Table 3 to form a group of variables for radiative transfer model input. This operation is repeated 500 times. Each time, we choose 25 further values of IWP (varying from 0 to 1000 g m^{-2}) and 15 values of D_{mm} (varying from 50 to 1000 μm), totaling 187 500 model runs for each frequency and each cloud class.

The brightness temperatures from these perturbed model runs are used to retrieve IWP and D_{mm}, and the retrievals are compared with the true values (model inputs) to assess the retrieval error. The errors are expressed here as percentage rms error and are shown in Figs. 9–12 for midtop ice cloud, midtop mixed-phase cloud, cirrus, and cirrus overlaying a lower liquid water cloud. For all the cloud classes, the maximum percentage rms error occurs when IWP and D_{mm} are both small. For IWP $<$ 200 g m^{-2} and $D_{mm} < 200$ μm, the retrieval errors for both IWP and D_{mm} are more than 50% for any cloud class, and increase rapidly with decreasing values of IWP or D_{mm}. Liquid water clouds are particularly troublesome to the retrievals when the ice clouds are at the same altitude as the liquid clouds (Fig. 10). For the midtop mixed-phase clouds, the IWP retrievals are no better than 75% accurate, and no better than 50% for D_{mm} over most of the ranges of IWP and D_{mm}. The retrieval accuracy significantly improves for cirrus overlaying a lower liquid water cloud (Fig. 12). Comparing the errors for the two ice only classes (Figs. 9 and 11), it is shown that the retrievals are more accurate when the ice cloud is located at higher altitude. This difference is considered to be caused mostly by uncertainties in water vapor. There is more water vapor between the ice cloud and the sensor (MIR) when the ice cloud locates at a lower altitude. Therefore, the water vapor uncertainty causes a bigger error for low ice clouds.

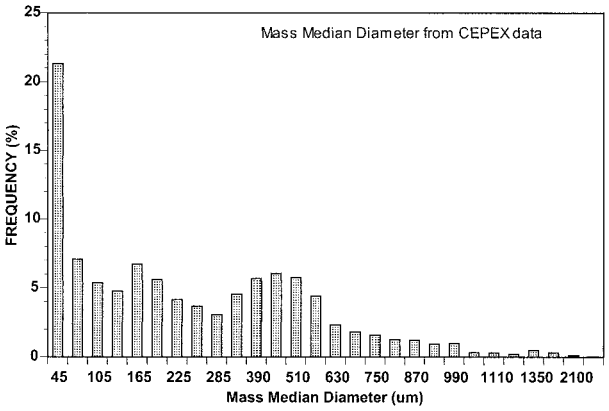

FIG. 8. Frequency distribution of D_{mm} computed from all available CEPEX microphysical data.

The simultaneous retrieval of IWP and D_{mm} is best suited to cirrus and cirrus overlaying a lower liquid water cloud (Figs. 11 and 12). Except for clouds with small values of IWP and D_{mm}, a better than 50% retrieval accuracy is expected for these two cloud classes. Clouds

TABLE 3. Uncertainties of variables used in the error analyses.

Variables	Uncertainty range
150-GHz T_B noise	$\pm$1 K
220-GHz T_B noise	$\pm$1 K
Cloud liquid water path	$\pm$100 g m^{-2}
Air temperature	$\pm$1°C
Precipitable water	$\pm$10 kg m^{-2}
Ice cloud height	$\pm$2 km
Surface wind speed	$\pm$4 m s^{-1}

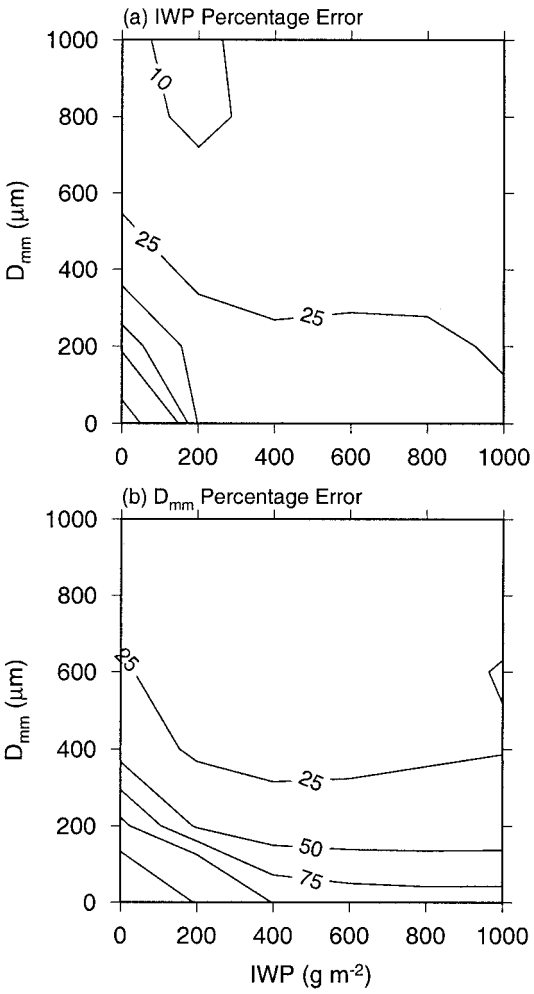

FIG. 9. Percentage rms error distributions of (a) IWP and (b) D_{mm} retrievals for midtop ice clouds. Contours are 5%, 10%, 25%, 50%, 75%, 100%, and 200%.

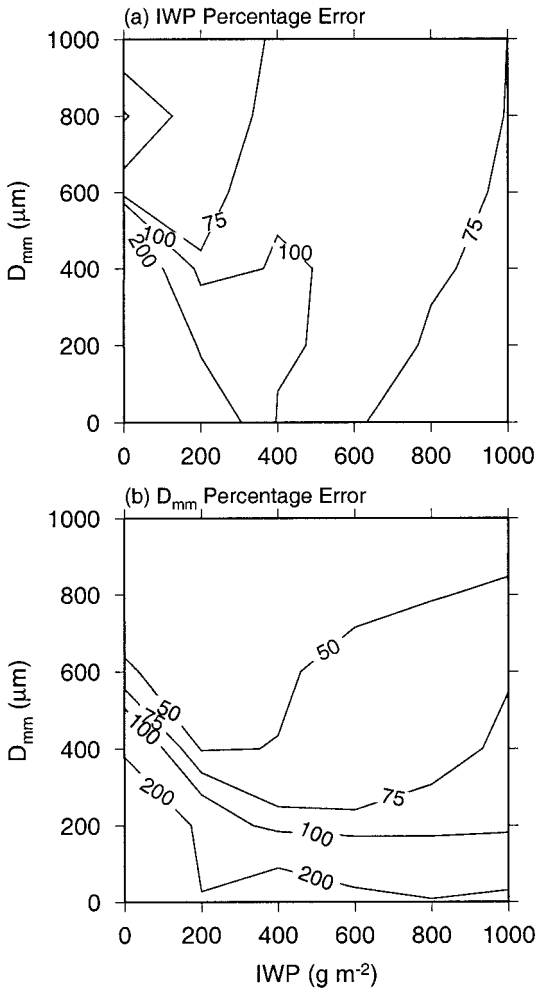

FIG. 10. Same as Fig. 9 but for midtop mixed-phase cloud.

with IWP < 200 g m^{-2} and $D_{mm} < 200$ μm are not suitable for the simultaneous retrievals using the 150- and 220-GHz channels. Combinations of higher frequencies are needed to resolve these thin clouds. In section 3, we used a statistical method to retrieve IWP for the low IWP and small D_{mm} clouds.

Another possible error, which may be significant but is not included in the aforementioned analysis, is due to the effect of particle shape. As mentioned in section 2, there could be many particle shapes within a single radiometer viewing volume, making it impractical to retrieve particle shape even when there were enough frequencies and polarizations. Deeter and Evans (2000) assessed this particle shape effect assuming that the ice particles are double overlapping prolate spheroids with similar aspect ratio to the 2DC images in CEPEX data. Based on radiative transfer model results, the irregularity of particle shapes increases the errors for both particle size and IWP retrievals by up to 60% compared to those for ice spheres. They concluded that particle shape uncertainty dominates the retrieval errors. It must be cautioned that their estimates are still preliminary. More investigations in the future are apparently needed. Similarly, better treatments of ice particle density and better ways to calculate the refractive index of nonsolid ice are also challenges for further improvement of the ice retrieval algorithm.

The uncertainty in water vapor profile, particularly for the upper troposphere, could be another error source. In the aforementioned error study, we varied water vapor amount at a certain altitude proportional to the absolute water vapor density at the same level at which we perturbed precipitable water. Because the majority of water vapor is confined in the lower atmosphere, this procedure may have underestimated the effect of water vapor uncertainty. Additionally, surface emissivity models for windy conditions at high microwave frequencies have not been well established so far. Although this uncertainty is not as serious in the Tropics as in higher latitudes because of the low wind conditions, more investigations are certainly needed in future studies. The al-

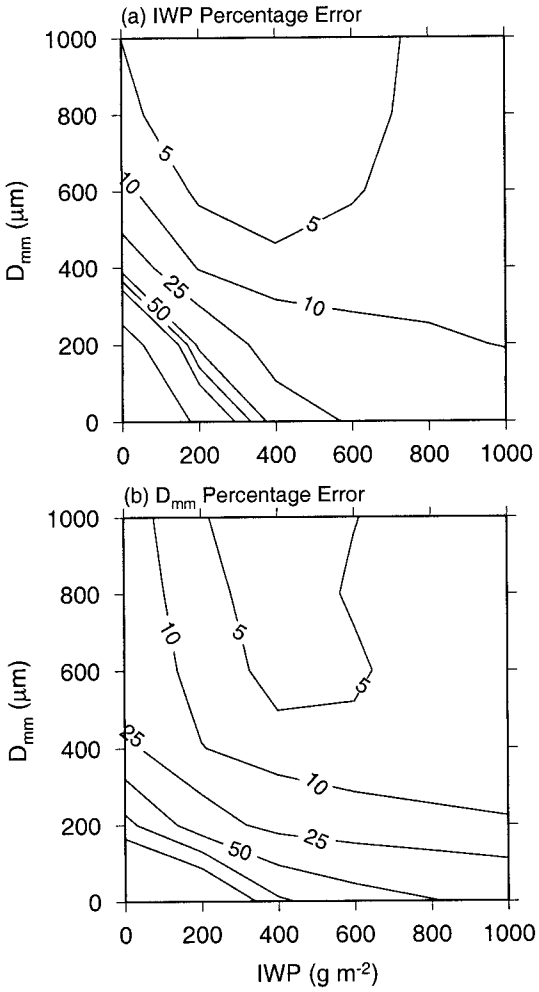

FIG. 11. Same as Fig. 9 but for cirrus.

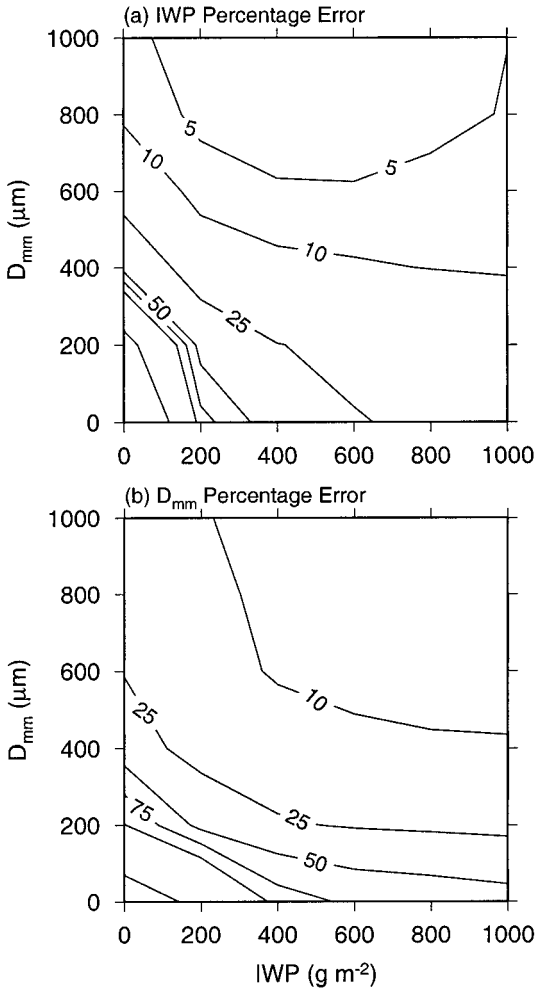

FIG. 12. Same as Fig. 9 but for cirrus overlaying a lower liquid water cloud.

gorithm proposed in this study is under the assumption of clouds over ocean. Emissivity over land is more complicated, mostly because of vegetation, wetness, and roughness. Therefore, retrieval error over land is expected to be larger than over ocean.

5. Conclusions

The method of simultaneous retrieval of ice water path and mass median diameter using microwave data at two frequencies is examined and implemented for tropical clouds. In developing the retrieval algorithm, we first derived a bulk mass–size relation for ice particles in tropical clouds using microphysical data collected during CEPEX. This relation effectively allows ice particle density to decrease with particle size, which is consistent with observational evidence. The ice particle size distribution is also derived from CEPEX data. A mass median diameter is used to vary the pattern of the size distribution. These CEPEX data–derived relations make it more suitable for the current algorithm to be applied to tropical ice clouds. MIR data at 150 and 220 GHz collected during TOGA COARE are used to implement the retrieval algorithm. An observed pixel is first classified by cloud type based on cloud-top temperature, liquid water path, and the presence of rain. In the current study, we limited the retrieval to four cloud classes: midtop ice cloud, midtop mixed-phase cloud, cirrus, and cirrus overlaying a lower liquid water cloud. Only nonprecipitating clouds are considered. In the retrieval algorithm, ice water path and mass median diameter are determined based on a lookup table, which is generated by a fast radiative transfer model and depends on cloud type, cloud liquid water path, atmospheric profiles and so on. In generating the lookup table, atmospheric profiles from ECMWF and liquid water path retrieval from AMPR data are incorporated.

Error analyses were performed using a Monte Carlo procedure in which atmospheric profiles, ice cloud height, liquid water content, surface temperature, and instrument noise vary randomly within their uncertainty

ranges through a Latin hypercube sampling scheme. The rms error in the retrievals is then assessed and presented in a two-dimensional diagram of ice water path and mass median diameter. It is shown that the simultaneous retrieval method using 150 and 220 GHz may be used for clouds with ice water path larger than 200 g m^{-2} and mass median diameter larger than 200 μm. To obtain meaningful retrievals for thinner ice clouds, higher microwave frequencies are needed. It is also shown that liquid water clouds that are at the same altitude of ice clouds seriously interfere with the retrievals of IWP. To obtain reasonable ice water path and mass median size retrievals, it is necessary first to group clouds into several classes, then to apply separate algorithm to different classes. The accuracy of the retrievals also depends on cloud type, with the best accuracy for cirrus and the worst for the midtop mixed-phase cloud among the cloud types investigated in this study.

IWP and D_{mm} frequency distributions were calculated using the retrieval algorithm. The simultaneous retrieval algorithm (2D retrieval) cannot be applied to the majority of the ice cloud pixels (Table 1), because the error becomes too large when $D_{mm} < 200$ μm and IWP $<$ 200 g m^{-2} and thin clouds dominate the cloud population. For this reason, the peak frequency near IWP $=$ 0, as shown by earlier investigators (Lin and Rossow 1996; Liu and Curry 1998, 1999), can be reproduced only after the data missed by the 2D retrieval algorithm are also accounted for. In this study, we retrieved IWPs for these thin clouds using a statistical method developed by Liu and Curry (1998). In addition, algorithms using visible/infrared data (e.g., Minnis et al. 1993a,b) may be more effective in deriving IWP and D_{mm} for thin cirrus clouds. Combining data from visible, infrared, and microwave wavelengths, or addition of submillimeter channels or active sensors such as lidar and radar, seems to be the future in ice water path retrievals.

Acknowledgments. The authors thank Jim Wang of NASA for providing MIR data through the TOGA COARE project, and Andy Heymsfield and Greg McFarquhar of NCAR for providing PMS 2DC data through CEPEX project. Discussions with Frank Evans while conducting this research were very helpful. Comments and suggestions from three anonymous reviewers were helpful for improving the quality of this paper, particularly the error analysis section. This research has been supported by NSF Grants ATM-9525801 and ATM-9910640, and NASA Grant NAG5-8647.

REFERENCES

Deeter, M. N., and K. F. Evans, 2000: A novel ice-cloud retrieval algorithm based on the Millimeter-Wave Imaging Radiometer (MIR) 150- and 220-GHz channels. *J. Appl. Meteor.,* **39,** 623–633.

Ebert, E. E., and J. A. Curry, 1992: A parameterization of ice cloud optical properties for climate models. *J. Geophys. Res.,* **97,** 970–978.

Evans, K. F., and G. L. Stephens, 1995a: Microwave radiative transfer through clouds composed of realistically shaped ice crystals. Part I: Single scattering properties. *J. Atmos. Sci.,* **52,** 2041–2057.

——, and ——, 1995b: Microwave radiative transfer through clouds composed of realistically shaped ice crystals. Part II: Remote sensing of ice clouds. *J. Atmos. Sci.,* **52,** 2058–2072.

——, S. J. Walter, A. J. Heymsfield, and M. N. Deeter, 1998: Modeling of submillimeter passive remote sensing of cirrus clouds. *J. Appl. Meteor.,* **37,** 184–205.

Fu, Q., and K. N. Liou, 1993: Parameterization of the radiative properties of cirrus clouds. *J. Atmos. Sci.,* **50,** 2008–2025.

Gasiewski, A. J., 1992: Numerical sensitivity analysis of passive EHF and SMMW channels to tropospheric water vapor, clouds, and precipitation. *IEEE Trans. Geosci. Remote Sens.,* **30,** 859–870.

Heymsfield, A. J., 1993: Microphysical structures of stratiform and cirrus clouds. *Aerosol–Cloud–Climate Interactions,* P. V. Hobbs, Ed., Academic Press, 97–121.

——, and L. J. Donner, 1990: A scheme for parameterizing ice-cloud water content in general circulation models. *J. Atmos. Sci.,* **47,** 1865–1877.

——, and G. M. McFarquhar, 1996: On the high albedos of anvil cirrus in the tropical Pacific warm pool: Microphysical interpretations from CEPEX. *J. Atmos. Sci.,* **53,** 2401–2423.

——, K. M. Miller, and J. D. Spinhirne, 1990: The 27–28 October 1986 FIRE IFO cirrus case study: Cloud microstructure. *Mon. Wea. Rev.,* **118,** 2313–2328.

King, M. D., and Coauthors, 1996: Airborne scanning spectrometer for remote sensing of cloud, aerosol, water vapor, and surface properties. *J. Atmos. Oceanic Technol.,* **13,** 777–794.

Klein, L. A., and C. T. Swift, 1977: An improved model for the dielectric constant of sea water at microwave frequencies. *IEEE Trans. Antennas Propag.,* **25,** 104–111.

Knollenberg, R. G., K. Kelly, and J. C. Wilson, 1993: Measurements of high number densities of ice crystals in the tops of tropical cumulonimbus. *J. Geophys. Res.,* **98,** 8639–8664.

Lin, B., and W. B. Rossow, 1994: Observations of cloud liquid water path over oceans: Optical and microwave remote sensing methods. *J. Geophys. Res.,* **99,** 20 907–20 927.

——, and ——, 1996: Seasonal variation of liquid water and ice water path in nonprecipitating clouds over oceans. *J. Climate,* **9,** 2890–2902.

Liou, K.-N., 1986: Influence of cirrus clouds on weather and climate processes. *Mon. Wea. Rev.,* **114,** 1167–1199.

Liu, G., 1998: A fast and accurate model for microwave radiance calculations. *J. Meteor. Soc. Japan,* **76,** 335–343.

——, and J. A. Curry, 1993: Determination of the characteristic features of cloud liquid water from satellite microwave measurements. *J. Geophys. Res.,* **98,** 5069–5092.

——, and ——, 1998: Remote sensing of ice water characteristics in tropical clouds using aircraft microwave measurements. *J. Appl. Meteor.,* **37,** 337–355.

——, and ——, 1999: Tropical ice water amount and its relations to other atmospheric hydrological parameters as inferred from satellite data. *J. Appl. Meteor.,* **38,** 1182–1194.

——, ——, and R.-S. Sheu, 1995: Classification of clouds over the western equatorial Pacific Ocean using combined infrared and microwave satellite data. *J. Geophys. Res.,* **100,** 13 811–13 826.

Matrosov, S. Y., T. Uttal, J. B. Snider, and R. A. Kropfli, 1992: Estimation of ice cloud parameters from ground-based infrared radiometer and radar measurements. *J. Geophys. Res.,* **97,** 11 567–11 574.

——, B. W. Orr, R. A. Kropfli, and J. B. Snider, 1994: Retrieval of vertical profiles of cirrus cloud microphysical parameters from Doppler radar and infrared radiometer measurements. *J. Appl. Meteor.,* **33,** 617–626.

McFarquhar, G. M., and A. J. Heymsfield, 1996: Microphysical characteristics of three cirrus anvils sampled during the Central Equatorial Pacific Experiment (CEPEX). *J. Atmos. Sci.,* **53,** 2424–2451.

McKay, M. D., R. J. Beckman, and W. J. Conover, 1979: A com-

parison of three methods for selecting values of input variables in the analysis of output from a computer code. *Technometrics,* **21,** 239–245.

Minnis, P., K. N. Liou, and Y. Takano, 1993a: Inference of cirrus cloud properties from satellite-observed visible and infrared radiances. Part I: Parameterization of radiance fields. *J. Atmos. Sci.,* **50,** 1279–1304.

——, P. W. Heck, and D. F. Young, 1993b: Inference of cirrus cloud properties from satellite-observed visible and infrared radiances. Part II: Verification of theoretical radiative properties. *J. Atmos. Sci.,* **50,** 1305–1322.

Mitchell, D. L., 1996: Use of mass- and area-dimensional power laws for determining precipitation particle terminal velocities. *J. Atmos. Sci.,* **53,** 1710–1723.

Pruppacher, H. R., and J. D. Klett, 1997: *Microphysics of Clouds and Precipitation.* Kluwer Academic, 954 pp.

Racette, P., R. F. Adler, J. R. Wang, A. J. Gasiewski, D. M. Jackson, and D. S. Zacharias, 1996: An airborne millimeter-wave imaging radiometer for cloud, precipitation, and atmospheric water vapor studies. *J. Atmos. Oceanic Technol.,* **13,** 610–619.

Schluessel, P., and H. Luthardt, 1991: Surface wind speeds over the North Sea from Special Sensor Microwave/Imager. *J. Geophys. Res.,* **96,** 4845–4853.

Sheu, R.-S., J. A. Curry, and G. Liu, 1997: Vertical stratification of tropical cloud properties as determined from satellite. *J. Geophys. Res.,* **102,** 4231–4245.

Spencer, R. W., R. E. Hood, F. J. LaFontaine, E. A. Smith, R. Platt, J. Galliano, V. L. Griffin, and E. Lobal, 1994: High-resolution imaging of rain systems with the Advanced Microwave Precipitation Radiometer. *J. Atmos. Oceanic Technol.,* **11,** 849–857.

Wang, J. R., J. Zhan, and P. Racette, 1997: Storm-associated microwave radiometric signatures in the frequency range of 90–220 GHz. *J. Atmos. Oceanic Technol.,* **14,** 13–31.

——, P. Racette, J. D. Spinhirne, K. F. Evans, and W. D. Hart, 1998: Observations of cirrus clouds with airborne MIR, CLS, and MAS during SUCCESS. *Geophys. Res. Lett.,* **25,** 1145–1148.

Webster, P. J., and R. Lukas, 1992: TOGA COARE: The Coupled Ocean–Atmosphere Response Experiment. *Bull. Amer. Meteor. Soc.,* **73,** 1377–1416.

Weng, F., and N. C. Grody, 1998: Two-stream approximation for microwave radiative transfer: Applications to satellite remote sensing of ice clouds. Preprints, *Ninth Conf. on Satellite Meteorology and Oceanography,* Paris, France, Amer. Meteor. Soc., 698–701.